Received: 19 February 2018 | Revised: 1 May 2018 | Accepted: 6 May 2018

DOI: 10.1111/cid.12645

WILEY

ORIGINAL ARTICLE

Modeling the effect of osseointegration on dental implant pullout and torque removal tests

Daniel Rittel PhD | Avraham Dorogoy PhD | Keren Shemtov-Yona DMD, PhD

Technion, Faculty of Mechanical Engineering, 32000, Haifa, Israel

Correspondence
Daniel Rittel, Technion, Faculty of Mechanical Engineering, 32000 Haifa, Israel.
Email: merittel@technion.ac.il

Abstract

Background: Osseointegration of dental implants is a key factor for their success. It can be assessed either by destructive (eg, pullout or torque extraction), or nondestructive methods (eg, resonant frequency analysis). However, as of today there is a scarcity of models that can relate the outcome of destructive tests to the level of osseointegration.

Purpose: To study various percentages of bone to implant bonding (tie) using finite element simulations. While evolutions of the bone mechanical properties are not explicitly taken into account, emphasis is put on the 3-dimensional variable extent of the bone-implant bonding, its statistical distribution, and its influence on the measurable extraction and torque loads, seeking to obtain a quantitative relationship.

Materials and Methods: We performed numerical simulations of randomly tied implants and calculated the evolution of the pullout force as well as that of the extraction torque.

Conclusion: Within simplifying assumptions for the osseointegration represented by a tie (as opposed to frictional) constraint, the results of this work indicate that the torque test is more discriminant than the extraction one, while both cannot really discriminate osseointegration levels below a relative variation of 20%.

KEYWORDS

dental implants, finite element, osseointegration, pullout, torque

1 | INTRODUCTION

The biological process of osseointegration has several definitions, of which the more practical was proposed by,[1,2] who used the term "functional ankylosis" to describe the rigid fixation of the implant to the jaw bone, and stated that "new bone is laid down directly upon the implant surface".

This ankylosis or anchorage evolves during the bone healing process following implant placement, during which new bone apposition is increasingly laid onto the implant surface, thus providing the "secondary stability" or rigid fixation of the implant to the bone.

Osseointegration may be evaluated scientifically by two objective ways. The bone-implant contact value (%BIC value), a histological term, expresses the percentage of implant surface in direct contact with the mineralized bone as determined from 2-dimensional histological sections. The second method consists of measuring the removal torque value that represents the mechanical interlocking between the implant and the surrounding bone. This test provides indirect information on the degree of BIC of a given implant. The RT value has been correlated with histologic assessments in animal studies.[3,4] Both methods are invasive, requiring implant removal, and thus are of limited clinical practicality and essentially used for research purposes.[5,6]

The time needed for secondary stability establishment is affected by several variables. Berglundh et al.[7] showed that implants subjected to 10 months of functional loading had more direct bone-implant contact than their unloaded counterparts. Based on the radiographic and histologic results, the study demonstrated that functional loading of implants may enhance osseointegration and increase the direct bone-implant contact.

In addition, several studies showed that the degree of surface roughness also influences the bone reactions to the applied load.[8,9]

Trisi et al.[10] evaluated the effect of 2 different thread designs on secondary stability (micromotion) and osseointegration rate in dense and cancellous bones. Secondary stability was assessed by measuring micromobility with a digital micrometer, reverse torque test and % BIC. Implants in dense bone reached higher secondary stability than those in cancellous bone, despite the lower %BIC. This study showed

that the key factors for implants secondary stability are the bone density (strength) and implant geometry (see also[11–13]).

From this brief literature review, it is clear that the amount of osseointegration can be fairly identified, but none of the studies dealing with bone-implant contact determination actually addressed the *quality* (eg, strength) of the bonding,[3] nor its correlation with implant stability. This point is clearly addressed in,[4,14] who mention several methods to assess the local properties of the peri-implant bone layer over, for example, a couple 100 microns, of which nanoindentation, albeit destructive, is the most direct determination method. Moreover, there is a lack of quantitative knowledge about how much secondary stability is sufficient to safely support occlusal load, so that a high degree of BIC is broadly considered as beneficial, without emphasis on the minimal required degree of BIC, not to mention the interfacial strength of the contact.

Finite element (FE) modeling has been used to assess dental implants secondary stability and/or the mechanical behavior of the jaw bone as a result of the loads prescribed by the implant (see eg, [15–17]) Those studies usually focused on bone-implant interfacial properties, when the interface was characterized by a specific strength, failure strain, and damage model,[15] or in fewer cases by a coefficient of friction by, for example, [18,19] Those studies did not address specifically the *3-dimensional geometrically random nature of the bone to implant attachment*, except for limited ex vivo studies as.[20]

In this work, we study various percentages of bone to implant bonding (tie) using numerical FE simulations. While evolutions of the bone mechanical properties are not explicitly taken into account, emphasis is put on the 3-dimensional variable extent of the bone-implant bonding, and its influence on the measurable extraction and torque loads, seeking to obtain a quantitative relationship.

2 | MATERIALS AND METHODS

The extraction of a representative commercial implant from the mandible bone was simulated numerically using the commercial FEs package Abaqus FE commercial package.[21] The model, [22] (see Supporting Information Appendix, Figure A1,) is 3-dimensional and the analyses are dynamic, continuous, and nonlinear. Two extraction procedures were modeled:

1. Straight implant pullout (pullout),
2. Reverse torque test/Rotational unscrewing.

2.1 | Pullout and unscrewing of partially bonded titanium alloy implant

2.1.1 | Assembly

The full assembly (Figure 1A, C) is comprised of three separate parts: (1) Mandible bone. (2) Implant. (3) Rigid screwdriver.

The assembly for *pullout* is shown in Figure 1A and does not include a screwdriver. The upward vertical load is applied on the inner face shown in Figure 1B.

The assembly for unscrewing (torque extraction) is shown in Figure 1C and includes all three parts. Unscrewing is done by applying a combined rotational velocity and a small vertical load. The

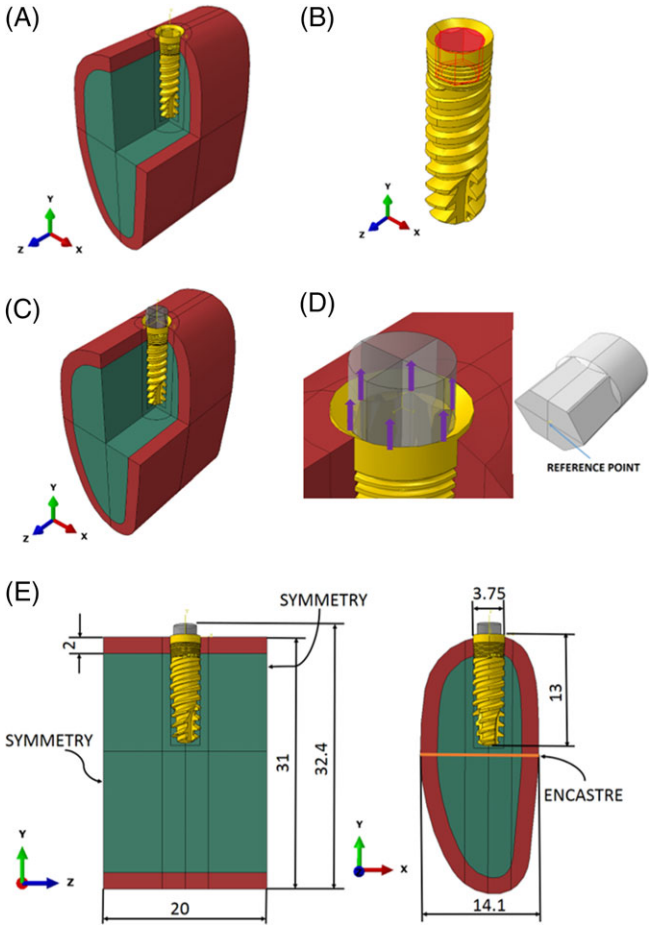

FIGURE 1 The assembly at the beginning of the pullout and unscrewing processes. A, Isometric view of the pullout assembly. B, The implant with the marked inner faces on which vertical displacements were applied. C, Isometric view of the unscrewing assembly. D, The screwdriver with its reference point location and the location of the vertical loads during unscrewing. E, Z-Y and X-Y side Z-Y side views with dimensions in mm. Note that "encastre" is the Abaqus terminology for fully constrained

counterclockwise rotational velocity is applied on the reference point of the rigid screwdriver. For this process, a vertical concentrated force of 1 N is applied at six locations on the upper face of the implant (Figure 1D), totaling a value of 6 N. The overall dimensions of the assembly are shown in Figure 1E.

2.1.2 | Material properties

The material properties used in this study are identical to those mentioned in previous numerical studies.[22] Consequently, they will only be briefly detailed here.

2.1.3 | Implant

For the sake of simplicity, the implant was modeled as an elastic isotropic material (Ti6Al4V), with properties listed in Table 1.

2.1.4 | Cortical bone

The cortical bone was modeled as an elastic-(almost) perfectly plastic material with Drucker-Prager pressure-sensitive behavior, as detailed in.[22] Ductile failure with damage evolution[23] was used as a failure

TABLE 1 Material Properties of Ti6Al4V

Density ρ (kg/m^3)	Young's modulus E (MPa)	Poisson's ratio, ν	Yield stress σ_Y (MPa)
4430	11 380	0.342	880

criterion. The plastic strain at fracture was set to 1% in tension and 2% in compression.[24] The "damage evolution value", was set to zero assuming abrupt failure of the cortical bone (Table 2).

2.1.5 | Cancellous bone

The cancellous bone is a cellular material[25] and is approximated here by an elastic-(almost ideal) plastic material model,[26–30] with its properties listed in Table 2.

2.1.6 | Screwdriver

The screwdriver was modeled as a rigid (nondeformable) body.

2.1.7 | Mesh

The mesh is shown in Figure 2. The meshed assembly is shown in Figure 2A. Some parts of the model have been removed to reveal the inner mesh as well as the mesh of the implant and its surroundings. A detail of the mesh of the implant and its surrounding which have a dense mesh of .25 mm seed size is shown in Figure 2B. The mesh of the bone and implant is comprised of 482 640 linear tetrahedral elements of type C3D4. The implant is meshed with 56 022 elements.

2.1.8 | Boundary conditions

The assembly was fixed in space by applying fully constrained conditions on a line along the planes $n_z = \pm 1$ (Figure 1E). Symmetry conditions were applied to the faces $n_z = \pm 1$ (Figure 1E).

The general contact algorithm of Abaqus[23] was used for the contact between the bone and the implant. Frictional tangential behavior with the penalty formulation was adopted. The frictional Coulomb coefficient of friction was set to .61.[26,31] The contact model included element-based surfaces that can adapt to the exposed surfaces of the current nonfailed elements.

All the surfaces that may become exposed during the analysis, including faces that are originally in the interior of bone and implant were included in the contact model. We assumed that contact nodes still take part in the contact calculations even after all of the surrounding elements have failed. These nodes act as free-floating point masses that can experience contact with the active contact faces.[23]

A surface-to-surface contact frictional tangential behavior with an arbitrarily selected coefficient of friction .8 was adopted for the contact between the rigid screwdriver and the implant shown in Figure 1B.

During *pullout*, the rigid implant was only allowed to move in the upward *y* direction.

A displacement of 3 mm in .2 s was applied. A smooth step amplitude was used to slow application of the load initially (see Supporting Information Appendix Figure A2).

For the *unscrewing* process, a constant angular velocity of 30 rpm (counterclockwise) was applied to the reference point of the screwdriver (Figure 1D), combined with the aforementioned vertical force component of 6 N (Figure 1D). Previous work has shown that the actual rotational velocity has no influence of the calculated results, except for reducing the computational time.[32]

2.1.9 | Modeling osseointegration

It is assumed that the implant is extracted sufficiently long after insertion so that full geometrical contact exists between the outer surface of the implant and the bone, and the osseointegration process is occurring. In this work, osseointegration is represented by a tie constraint on the interface between the implant and the bone. In other words, tied elements correspond to infinite interfacial strength, so that bone-implant debonding occurs in the bone tissue around the interface. As such, it occurs over an area fraction of the fully contacting surfaces of the implant and bone. This area fraction varies, and is assumed to be *randomly* distributed over the whole peripheral contact area, be it for both the cortical and trabecular constituents, or separately. The relative osseointegrated area (ROA), ranging from 0% to 100%, is defined as: $ROA = \frac{A_{\text{osseointegration}}}{A_{\text{Implant outer surface}}}\ [\%]$.

The remaining 1-ROA percentage is assumed to have a frictional interaction with the implant, as described earlier, but the interfacial strength is zero.

3 | RESULTS

3.1 | Relative areas of the cortical and trabecular bone

The relative contact between the dental implant and the bone components varies with each implant geometry and bone structure. Given the complex geometry of typical dental implants, the contact areas of any implant can be extracted from the FE model.

Here, for the completely inserted implant in the modeled jawbone of this work, it was found that 30.12 mm^2 (16%) of the implant contact surface is in contact with the cortical bone, while the remaining 161.56 mm^2 (84%) is in contact with the trabecular. Keeping in mind that those figures represent the upper bound value of the contact areas (full insertion), those results are nevertheless important for the understanding of the forthcoming results.

TABLE 2 Mechanical and Failure Properties of the Bone Components

	Density ρ (kg/m^3)	Young's modulus E (MPa)	Poisson ratio ν	Yield stress σ_Y (MPa)	Drucker Prager β (°)	Fracture plastic strain tension ε_p^T(%)	Fracture plastic strain compression ε_p^C(%)	Damage evolution (μm)
Cortical bone	1900	18 000	0.35	180	30	1	2	0.0
Cancellous bone	1000	700	0.35	32	0	0.135	0.135	10

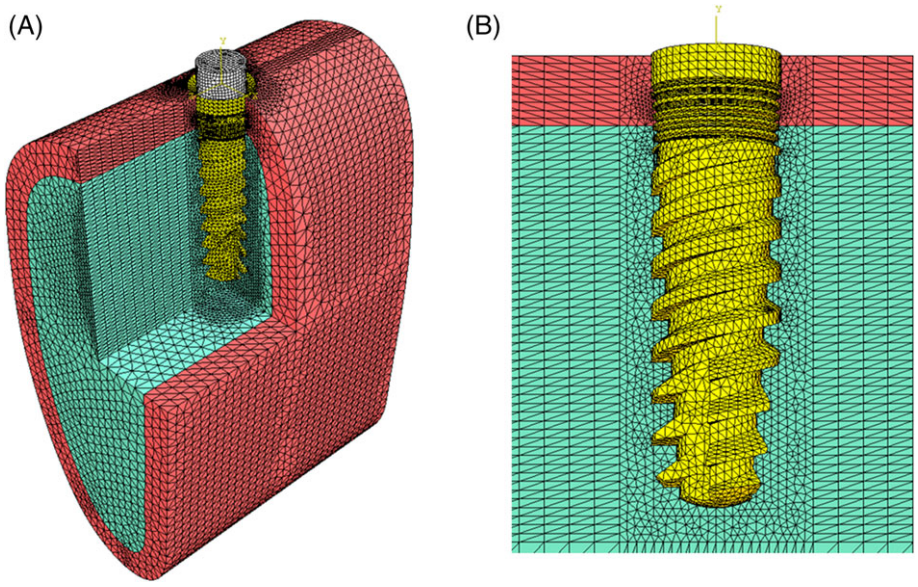

FIGURE 2 A, The meshed assembly. B, The exposed mesh near the implant

3.2 | Pullout of Ti6Al4V implant

Nine different ROA's were analyzed: 0%, 1.0%, 2.5%, 5.1%, 9.5%, 24%, 48.9%, 80.2%, and 100%, respectively. The elements on these osseointegrated areas were chosen *randomly*, as illustrated in Figure 3. Consequently, the values quoted for the ROA throughout this article are reported as calculated, and not rounded.

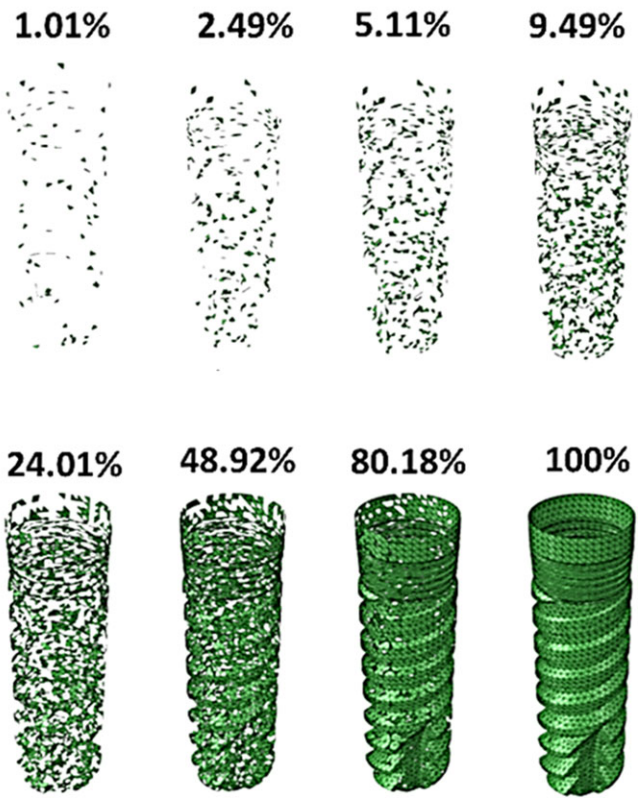

FIGURE 3 The randomly chosen areas on the outer surface of the implant in which osseointegration took place (ROA). A, 1%. B, 2.5%. C, 5.1%. D, 9.5%. E, 24%. F, 48.9%. G, 80.2. H, 100% (full bonding)

The resulting load-displacements curves corresponding to 7 representative case studies are shown in Figure 4.

The first result of those simulations is that the overall load-displacement characteristics of the pullout test are globally sensitive up to the first 5% of osseointegration, as an ROA of 9.5% cannot be distinguished from 100%. Beyond this value, the increasing percentage of osseointegration is not observed to influence the pullout curve. Those results suggest that the very initial stage of osseointegration is sufficient to firmly anchor the implant in the jawbone *vis a vis* vertical loads. Those results also indicate that the pullout test is not highly discriminative concerning the level of osseointegration.

Next, the effect of the random selection of the tied surfaces was independently assessed by running three different cases for a similar percentage, here ~5%. Supporting Information Appendix Figure A3A shows the different three sets of elements while Supporting Information Figure A3B shows the corresponding load-displacements curves.

From this limited study, it can be seen that as long as the random selection concerns the overall contacting bone (cortical and trabecular), the load-displacement curves are relatively identical, so that the previous conclusions concerning the pullout test can now be

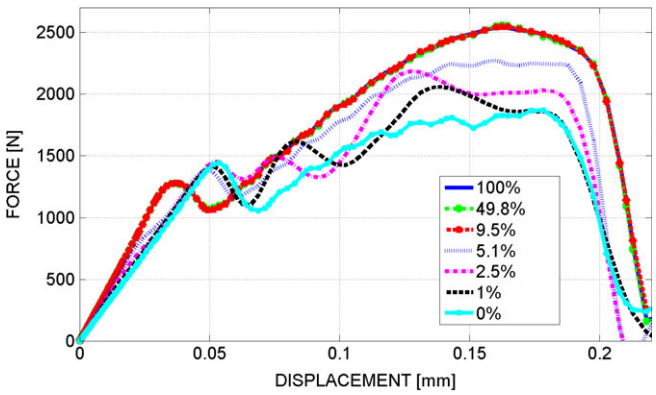

FIGURE 4 The smoothed load-displacement curves for pullout of a Ti6Al4V implant with different percentage of osseointegrated areas (ROA)

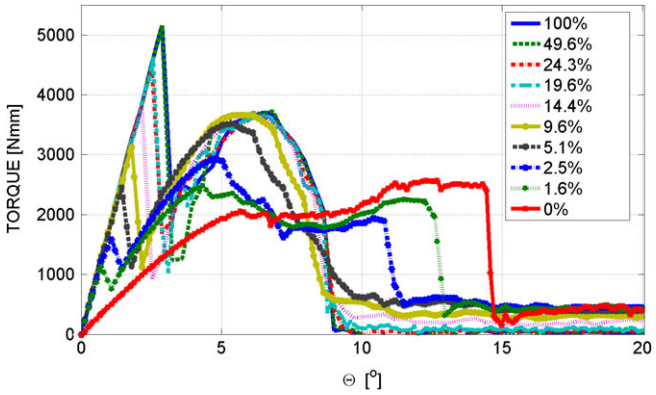

FIGURE 5 The torque-angle curves of unscrewing a Ti6Al4V implant with different ROA's

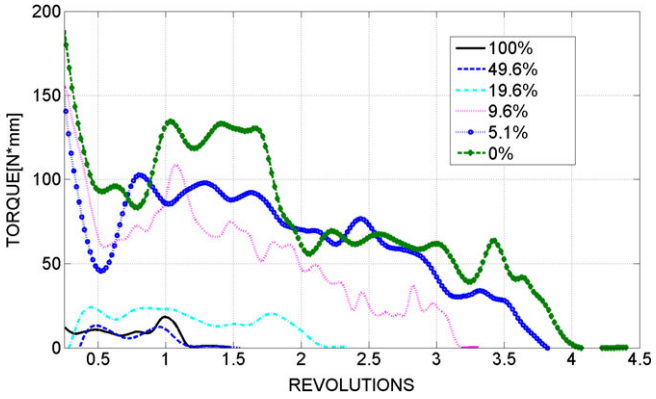

FIGURE 6 The smoothed "residual" torque for different ROA's vs the number of revolutions

generalized since they seem to be independent of the random selection process and location of the tied surface on either cortical or trabecular interfaces.

3.3 | Reverse torque test of Ti6Al4V implant

Ten different percentages of randomly chosen osseointegrated areas (ROA) were considered: 0%, 1.6%, 2.5%, 5.1%, 9.6%, 14.4%, 19.6%, 24.3%, 49.6%, and 100%, respectively. The torque presented here (Figure 5) is the reaction torque calculated at the reference point located on the rigid screwdriver.

Figure 5 shows that for all ROA, the resulting torque-angle relationships consist of three phases. The first phase is linear until a significant drop in the torque value, and it mostly involves the cortical bone. The second phase involves increasingly the trabecular bone component. It consists of a nonlinear torque-angle evolution that ends with very low residual constant values of the torque (onset of third phase). These low residual values are less than 25 Nmm for ROA > 24%. The first two phases are short and take place within the first 10°-15° of revolution. The third phase consist of the decreasing evolution of the residual torques for different ROA at high rotational angles in the range of ~$15^{\circ} \le \Theta \le 1620^{\circ}$. Figure 6 illustrates this evolution in the range $90^{\circ} \le \Theta \le 1620^{\circ}$. It can be observed that for all ROA's, the torque drops to zero, meaning that the implant is fully released and can move upward with no restraint due to the upward extraction force of 6 N (Figure 1D).

Figure 7A shows the implant release points, in which all the vertical displacements increase linearly until a marked change of slope illustrating the free final pullout. Until that point, the implant is unscrewed out within the remains of the damaged threads. For all ROA > 50% the torque drops to zero at 450° (1.25 revolutions), and further osseointegration does not affect the rotational angle at which the implant is fully released. As the ROA% decreases below 50%, the number of revolutions until implant release increases. Note that the case of ROA = 0% is fully released last after rotation of ~1470° (4.1 revolutions). Since the length of the implant is 13.5 mm, the horizontal line in Figure 10A indicates the location of the top face of the bone. Figures 7B, C show the location of the implant within the bone at full release for high and low ROA.

The number of revolutions to full release depends on the amount of damage caused to the bone threads during the first two phases of the extraction. For high ROA larger damage is caused, namely destruction of the bone threads (see Figure 8), and hence the implant is released at a lower number of revolutions.

Figure 8 shows the implant location and the bone plastic deformation at three distinct rotations: 7.2°, 72°, and 216°. It compares two cases: One of ROA = 100%, which is shown on the left and the other ROA = 5.1%, which is shown on the right. At an angle of ~7.2°,

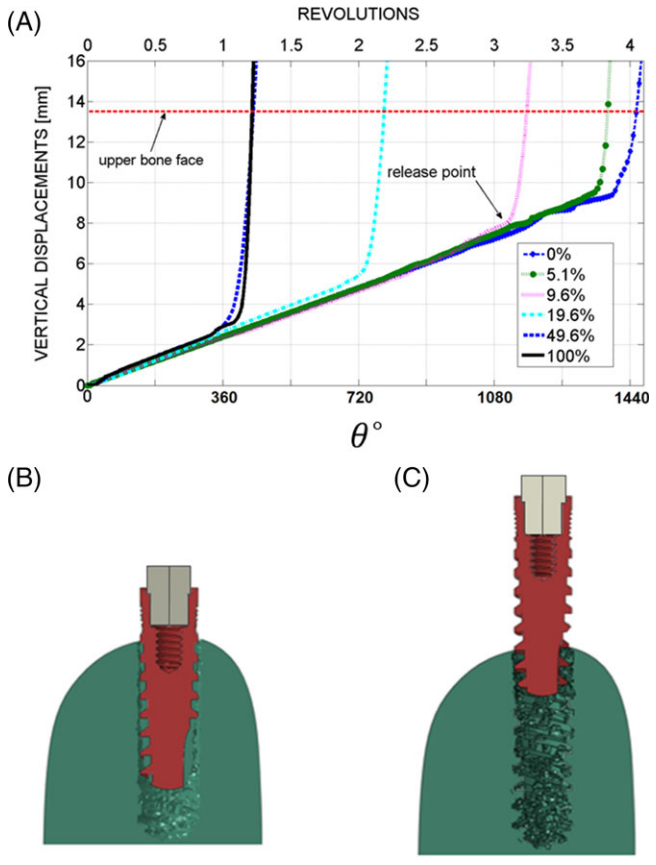

FIGURE 7 A, The vertical displacement for ROA = 0%, 5.1%, 9.6%, 19.6%, 49.6%, and 100% vs the number of implant revolutions. Note that at d = 13.5 the implant is fully exposed outside the bone. B, Location of the implant at full release for ROA = 100%. C, Location of implant at full release for ROA = 5.1%

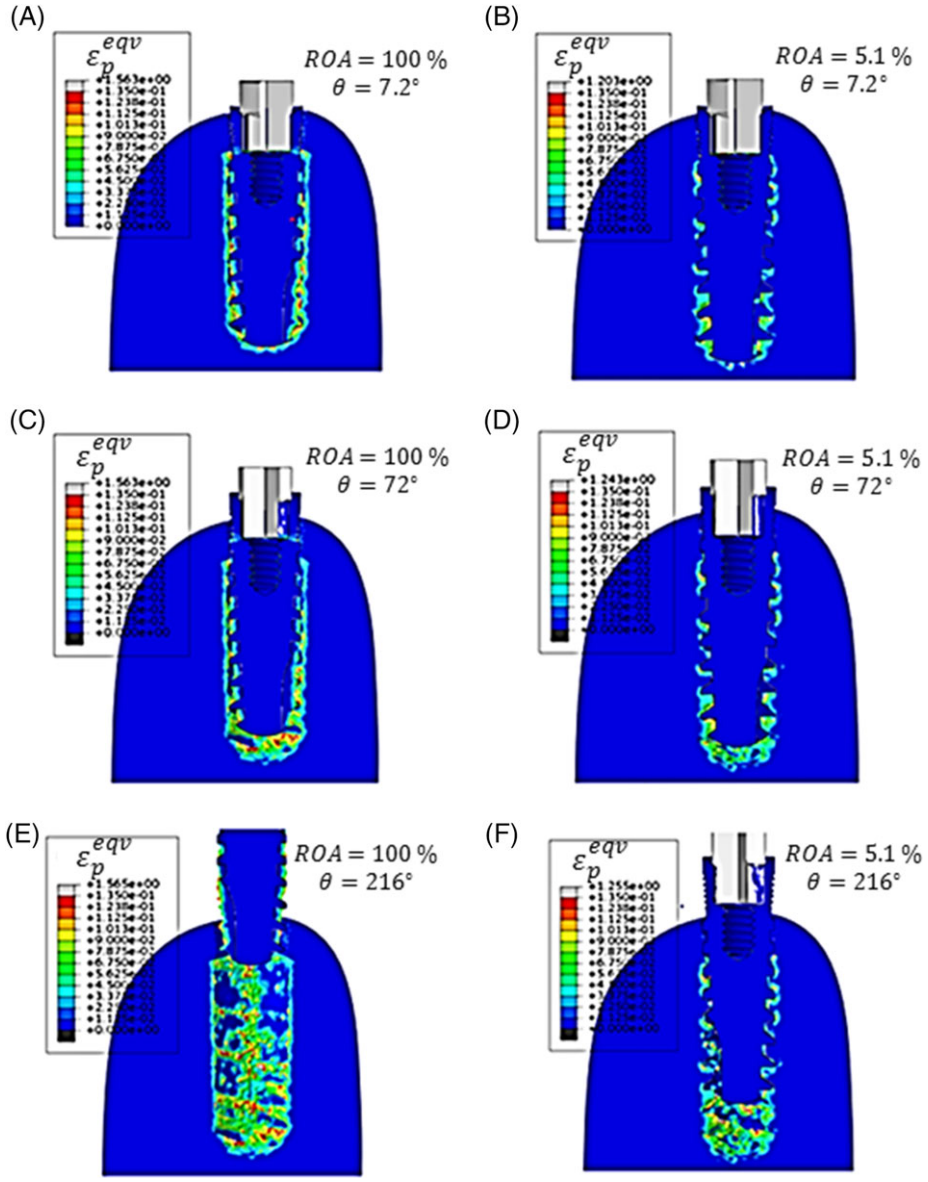

FIGURE 8 Implant location and bone plastic deformation (PEEQ)—comparison between ROA = 100% (left) to ROA = 5% (right) osseointegration for the same applied rotation: ⊖ = 7.2°, 72°, and 216°. Note the larger plastic deformations and the disappearance of the bone' threads for ROA = 100%

both extraction torques reach an extremum value which can be seen in Figure 6. At 72° both implants are detached from their initial state. At 216°, the difference in their vertical displacement is clearly visible.

3.4 | Effect of partial bonding in trabecular or cortical bone

So far, partial bonding was assumed to occur randomly on *both* cortical and trabecular bone components. Although we do not investigate preferential osseointegration in a specific component (as in eg, [33,34]), it is nevertheless of interest to consider each bone component separately. Consequently, in this section, the ROA was systematically and randomly varied over the cortical or the trabecular bone interface, while the complementary bone section underwent only frictional interaction without any bonding.

3.5 | Pullout of implant partially bonded to cortical bone alone and trabecular bone alone

The smoothed resisting force due to pulling, which is shown in Figure 9A, was calculated for 7 values of ROA: 2.6%, 5.3%, 10.1%, 21.1%, 49.6%, 73.6%, and 100% in the cortical bone. Here, the reported percentage is relative to the total area of the cortical bone (16%).

Figure 9B shows the smoothed resisting force, as calculated for 7 values of ROA: 2.5%, 5.2%, 9.9%, 20%, 49.6%, 74.9%, and 100%. Here, the reported percentage is relative to the total area of the trabecular bone (84%).

The comparison of Figure 9A, B shows that the peak loads in Figure 9B (trabecular) are higher by ~800 N from those of Figure 9A (cortical). The variations for all ROA in Figure 9A are similar, while in Figure 9B they are similar only for all ROA > 20%. As a consequence

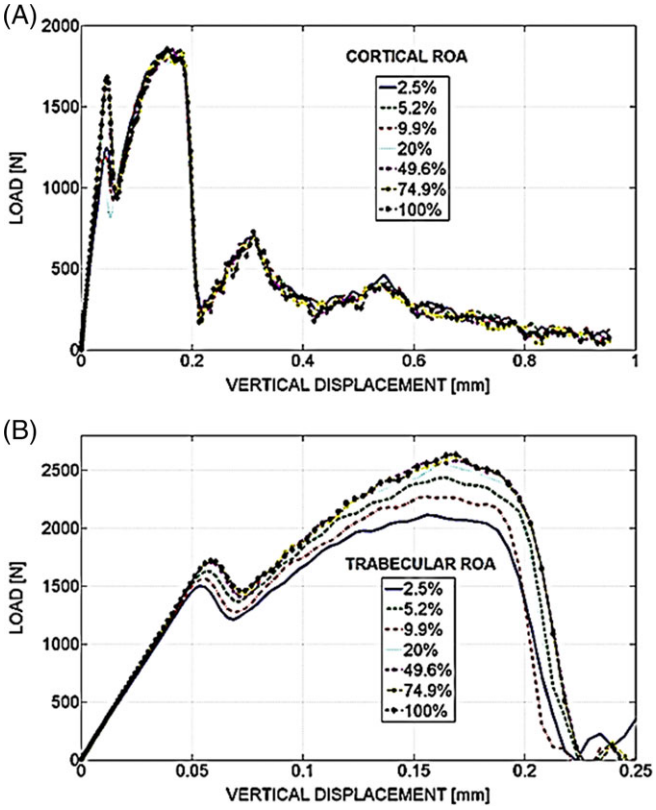

FIGURE 9 A, The extracting force due to different ROA of the cortical bone. B, The extracting force due to different ROA of the trabecular bone

the various ROA's of the cortical bone cannot be distinguished based on load-displacement, while for the trabecular bone, only ROA <20% can be distinguished. This may simply be the result of the relatively small area occupied by the cortical bone.

3.6 | Reverse torque test of implant partially bonded to cortical bone alone and trabecular bone alone

The resisting torque due to unscrewing, shown in Figure 10A, was calculated for 7 values of ROA in the cortical bone component and Figure 10B for the trabecular bone.

Here, one can notice that both the partially osseointegrated trabecular and cortical bone components make a distinguishable contribution to the torque-angle relationship. The peak torque values of the cortical bone are higher by ~600 Nmm from those of the trabecular bone. Both in Figure 10A, B, all curves for the range 20% < ROA < 100% coincide. Differences between the curves are observed only for ROA < 20%. In Figure 10A, the lower ROA cause less sharp peak at the initial angle of 1-2°, but increases the extremum at 5-6°. In Figure 10B, the lower ROA cause a lower resisting torque.

4 | DISCUSSION

The central issue of bone osseointegration has not been yet extensively modeled, and from a clinical point of view, there are only two approaches, one destructive (torque or pullout tests), the second being nondestructive (eg, RFA).

Yet, it is important to model those two destructive tests and see what exactly can be learned from them, all the more so in the absence of a standard procedure to estimate secondary stability of a dental implant.

Modeling osseointegration can be an extremely complex task if one considers the kinetics of the process. In this work, we adopted an original, albeit simplified, approach to osseointegration in which we assumed 100% geometrical contact, but randomly selected surfaces were either tied with an infinite strength or frictional without resistance. The kinetics of the process, namely the biological evolution, were left aside and osseointegration was considered as a binary process (osseointegration or not), whose evolution was quantified by the ROA percentage. One should note that the original 3-dimensional nature of this study reflects progress achieved by 3-dimensional imaging techniques (eg, CBT), as opposed to the more traditional 2-dimensional histologic characterization.

Yet, one must note that although the bone-implant geometrical contact was kept to 100% in all calculations, one can consider frictional interfaces as some kind on non (or weak) contacting faces. With that, it is clear that the *quality of the contact*, embodied here as an infinite interfacial strength, should be further addressed in future studies in order to increase the clinical relevance of such studies.

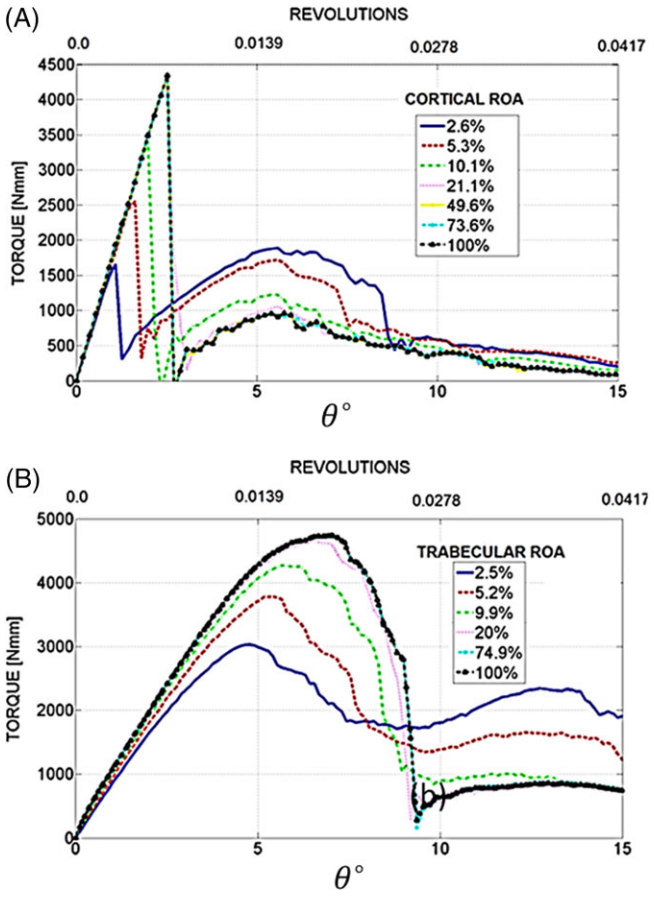

FIGURE 10 A, The resisting torque due to different ROA of the cortical bone. B, The resisting torque due to different ROA of the trabecular bone

The first important point is that we could show that the random location of the chosen tied (osseointegrated) surfaces does not affect the test results for a fixed osseointegrated percentage (ROA), thereby eliminating a potential influence of the random location of the tied elements on the contacting surfaces.

This preliminary phase also assessed the exact areas of trabecular and cortical bone components that are in contact with the implant. It is believed that such an assessment should be routinely carried out as part of the implant design and suitability, all the more so when empirical relations are sought between the implant diameter and fraction of bone to implant contact.

We separately modeled the pullout and the torque extraction tests. This was done in two distinct phases.

In the first phase of this investigation, we only considered random osseointegration over the whole implant surface without giving any preference to the bone component. In the second phase, we addressed selective osseointegration in the cortical or trabecular components alone. This point has not been considered so far in the literature, except to a limited extent, as in.[34] However, this study considered only the mechanical stiffness of the bone-implant system, as opposed to the whole extraction process modeled here, thereby precluding further detailed comparison. Yet, as noticed in previous works of a similar nature, both the cortical and the trabecular bone components have a definite contribution to the calculated loads or torques. The trabecular bone has a lower mechanical strength than cortical, but it can sustain higher strains to failure. The dominant role of the trabecular is now rationalized based also on the fact that its contact surface is much larger (by a factor of 5-6) than that of the cortical, thereby compensating for its lower strength.

The results of those calculations show first that, of the two mechanical tests, the pullout test is less discriminating than that the torque one.

But what is more interesting is the observation that past a certain low level of ROA (from 5% to 20% depending on the test), additional osseointegration cannot be screened by the tests. This observation is particularly interesting because of its clinical implications. The present observations show that high ROA, although preferable, cannot be distinguished by these tests alone, and that a much smaller ROA will confer early stability to the system, where stability is related to the maximum extraction torque or force. One could thus hypothesize that strong bonding over more than 20% of the bone-implant interfacial area can be considered as some sort of redundant constraint.

Finally, this study shows that the mechanical extraction test results depend on the *combined* relative contact area *and* the interfacial mechanical characteristics, and not solely to the area contact, as both factors determine the exact constraint applied to the implant. One can easily assume that both contact area and interfacial characteristics will therefore determine the implant micromotions that are often considered as a token of stability. Yet, a standard evaluation method that incorporates both factors and implant stability is still to be developed.

5 | CONCLUSIONS

- The relative contact area of any implant geometry with the bone components should be determined for better understanding the role of each bone component on the extraction process.
- The trabecular component has a higher contribution to the pullout force and extraction torque due to its high relative contact area.
- Neither pullout test or torque values can discriminate beyond a relatively low percentage of osseointegration (not exceeding 20%).
- The torque extraction test has a relative advantage over the pullout test in discriminating the percentage of osseointegration.
- Even a limited amount of osseointegration (ca. 20%) appears to be sufficient to confer secondary stability to a dental implant.
- Both contact area percentage and interfacial mechanical characteristics determine the implant stability.

CONFLICT OF INTEREST

The authors declare they have no conflict of interest.

ORCID

Daniel Rittel http://orcid.org/0000-0003-4458-9382

REFERENCES

1. Schroeder A, Pohler O, Sutter F. Tissue reaction to an implant of a titanium hollow cylinder with a titanium surface spray layer. *SSO Schweiz Monatsschr Zahnheilkd*. 1976;86:713-727.
2. Schroeder A, van der Zypen E, Stich H, Sutter F. The reaction of bone, connective tissue and epithelium to endosteal implants with sprayed titanium surfaces. *J Maxillofac Surg*. 1981;9:15-25.
3. Johansson C, Albrektsson T. A removal torque and histomorphometric study of commercially pure niobium and titanium implants in rabbit bone. *Clin Oral Imp Res*. 1991;2:24-29.
4. Haïat G, Wang H-L, Brunski J. Effects of biomechanical properties of the bone-implant Interface on dental implant stability: from in silico approaches to the Patient's mouth. *Annu Rev Biomed Eng*. 2014;16:187-213.
5. Steigenga J, Al-Shammari K, Misch C, Nociti FH, Wang H-L. Effects of implant thread geometry on percentage of Osseointegration and resistance to reverse torque in the tibia of rabbits. *J Periodontol*. 2004;75:1233-1241.
6. Gehrke SA, Marin GW. Biomechanical evaluation of dental implants with three different designs: removal torque and resonance frequency analysis in rabbits. *Ann Anat*. 2015;199:30-35.
7. Berglundh T, Abrahamsson I, Lindhe J. Bone reactions to longstanding functional load at implants: an experimental study in dogs. *J Clin Periodontol*. 2005;32:925-932.
8. Berglundh T, Abrahamsson I, Lang NP, Lindhe J. De novo alveolar bone formation adjacent to endosseous implants. A model study in the dog. *Clin Oral Implants Res*. 2003;14:251-262.
9. Gotfredsen K, Berglundh T, Lindhe J. Bone reactions adjacent to titanium implants subjected to static load of different duration. A study in the dog (III). *Clin Oral Implants Res*. 2001;12:552-558.
10. Trisi P, Berardini M, Falco A, Vulpiani MP. Effect of implant thread geometry on secondary stability, bone density, and bone-to-implant contact. *Implant Dent*. 2015;24:384-391. https://doi.org/10.1097/ID.0000000000000269.
11. Lin D, Li Q, Li W, Zhou S, Swain MV. Design optimization of functionally graded dental implant for bone remodeling. *Compos Part B Eng*. 2009;40:668-675.

12. Abuhussein H, Pagni G, Rebaudi A, Wang H-L. The effect of thread pattern upon implant osseointegration. *Clin Oral Implants Res*. 2010; 21:129-136.
13. Shibata Y, Tanimoto Y. A review of improved fixation methods for dental implants. Part I: surface optimization for rapid osseointegration. *J Prosthodont Res*. 2015;59:20-33.
14. Mathieu V, Vayron R, Richard G, et al. Biomechanical determinants of the stability of dental implants: influence of the bone-implant interface properties. *J Biomech*. 2014;47:3-13.
15. Doblaré M, García JM, Gómez MJ. Modelling bone tissue fracture and healing: a review. *Eng Fract Mech*. 2004;71:1809-1840.
16. Mellal A, Wiskott HWA, Botsis J, Scherrer SS, Belser UC. Stimulating effect of implant loading on surrounding bone. Comparison of three numerical models and validation by in vivo data. *Clin Oral Implants Res*. 2004;15:239-248.
17. Piccinini M, Cugnoni J, Botsis J, Ammann P, Wiskott A. Numerical prediction of peri-implant bone adaptation: comparison of mechanical stimuli and sensitivity to modeling parameters. *Med Eng Phys*. 2016; 38:1348-1359.
18. Rittel D, Dorogoy A, Shemtov-Yona K. Modelling dental implant extraction by pullout and torque procedures. *J Mech Behav Biomed Mater*. 2017;71:416-427.
19. Korabi R, Shemtov-Yona K, Dorogoy A, Rittel D. The failure envelope concept applied to the bone-dental implant system. *Sci Rep*. 2017; 7(2051):2051.
20. Hsu J-T, Shen Y-W, Kuo C-W, Wang R-T, Fuh L-J, Huang H-L. Impacts of 3D bone-to- implant contact and implant diameter on primary stability of dental implant. *J Formos Med Assoc*. 2017;116: 582-590.
21. Abaqus. *Finite Element Package (Explicit), v6*. 2014:14-12.
22. Dorogoy A, Rittel D, Shemtov-Yona K, Korabi R. Modeling dental implant insertion. *J Mech Behav Biomed Mater*. 2017;68:42-50.
23. Simulia. *Abaqus/Explicit Version 6.14-2*, *Abaqus documentation*. Providence, RI: Dassault Systemes Simulia Corporation, 2014.
24. Keaveny TM, Hayes WC. Mechanical properties of cortical and trabecular bone. *Bone*. 1992;285:344.
25. Ashby MF, Medalist RFM. The mechanical properties of cellular solids. *Metall Trans A*. 1983;14:1755-1769.
26. Guan H, van Staden RC, Johnson NW, Loo Y-C. Dynamic modelling and simulation of dental implant insertion process—a finite element study. *Finite Elem Anal Des*. 2011;47:886-897.
27. Gibson LJ. The mechanical behaviour of cancellous bone. *J Biomech*. 1985;18:317-328.
28. Van Staden RC, Guan H, Johnson NW, Loo Y, Meredith N. Step-wise analysis of the dental implant insertion process using the finite element technique. *Clin Oral Implants Res*. 2008;19:303-313.
29. Reilly DT, Burstein AH. The mechanical properties of cortical bone. *J Bone Jt Surg Am*. 1974;56:1001-1022.
30. TM K, WC H, Keaveny T, Hayes W. Mechanical properties of cortical and trabecular bone. *Bone*. 1992;285:344.
31. Grant JA, Bishop NE, Götzen N, Sprecher C, Honl M, Morlock MM. Artificial composite bone as a model of human trabecular bone: the implant-bone interface. *J Biomech*. 2007;40:1158-1164.
32. Dorogoy A, Rittel D, Shemtov-Yona K, Korabi R. Modeling dental implant insertion. *J Mech Behav Biomed Mater*. 2017;68:42-50.
33. Caroprese M, Lang NP, Rossi F, Ricci S, Favero R, Botticelli D. Morphometric evaluation of the early stages of healing at cortical and marrow compartments at titanium implants: an experimental study in the dog. *Clin Oral Implants Res*. 2017;28:1030-1037.
34. Ruffoni D, Wirth AJ, Steiner JA, Parkinson IH, Müller R, van Lenthe GH. The different contributions of cortical and trabecular bone to implant anchorage in a human vertebra. *Bone*. 2012;50:733-738.

SUPPORTING INFORMATION

Additional supporting information may be found online in the Supporting Information section at the end of the article.

How to cite this article: Rittel D, Dorogoy A, Shemtov-Yona K. Modeling the effect of osseointegration on dental implant pullout and torque removal tests. *Clin Implant Dent Relat Res*. 2018;1–9. https://doi.org/10.1111/cid.12645